J. Biochem. 131, 365–374 (2002)

Three-Dimensional Structure of the Flavoenzyme Acyl-CoA Oxidase-II from Rat Liver, the Peroxisomal Counterpart of Mitochondrial Acyl-CoA Dehydrogenase[1]

Yoshitaka Nakajima,* Ikuko Miyahara,* Ken Hirotsu,*[2] Yasuzo Nishina,† Kiyoshi Shiga,† Chiaki Setoyama,‡ Haruhiko Tamaoki,‡ and Retsu Miura‡

*Department of Chemistry, Graduate School of Science, Osaka City University, Sugimoto, Sumiyoshi-ku, Osaka 558-8585; and Departments of †Physiology and ‡Biochemistry, Kumamoto University, School of Medicine, Honjo, Kumamoto 860-0811

Received November 10, 2001; accepted December 8, 2001

Acyl-CoA oxidase (ACO) catalyzes the first and rate-determining step of the peroxisomal β-oxidation of fatty acids. The crystal structure of ACO-II, which is one of two forms of rat liver ACO (ACO-I and ACO-II), has been solved and refined to an *R*-factor of 20.6% at 2.2-Å resolution. The enzyme is a homodimer, and the polypeptide chain of the subunit is folded into the N-terminal α-domain, β-domain, and C-terminal α-domain. The X-ray analysis showed that the overall folding of ACO-II less C-terminal 221 residues is similar to that of medium-chain acyl-CoA dehydrogenase (MCAD). However, the N-terminal α- and β-domains rotate by 13° with respect to the C-terminal α-domain compared with those in MCAD to give a long and large crevice that accommodates the cofactor FAD and the substrate acyl-CoA. FAD is bound to the crevice between the β- and C-terminal domains with its adenosine diphosphate portion interacting extensively with the other subunit of the molecule. The flavin ring of FAD resides at the active site with its *si*-face attached to the β-domain, and is surrounded by active-site residues in a mode similar to that found in MCAD. However, the residues have weak interactions with the flavin ring due to the loss of some of the important hydrogen bonds with the flavin ring found in MCAD. The catalytic residue Glu421 in the C-terminal α-domain seems to be too far away from the flavin ring to abstract the α-proton of the substrate acyl-CoA, suggesting that the C-terminal domain moves to close the active site upon substrate binding. The pyrimidine moiety of flavin is exposed to the solvent and can readily be attacked by molecular oxygen, while that in MCAD is protected from the solvent. The crevice for binding the fatty acyl chain is 28 Å long and 6 Å wide, large enough to accommodate the C23 acyl chain.

Key words: acyl-CoA dehydrogenase, acyl-CoA oxidase, flavoenzyme, three-dimensional structure, X-ray crystallography.

Fatty acid β-oxidation systems are known to occur in mitochondria, peroxisomes, and bacteria. Mammalian acyl-CoA oxidase (ACO, EC 1.3.3.6) is a flavoenzyme that contains one molecule of noncovalently-bound FAD per subunit as the prosthetic group and catalyzes the initial and rate-determining step of the peroxisomal β-oxidation pathway. In the reductive half-reaction of ACO, the substrate acyl-CoA is α,β-dehydrogenated into the corresponding *trans*-enoyl-CoA by FAD, which becomes reduced, while in the oxidative half-reaction, reduced FAD is reoxidized by molecular oxygen, thereby closing the catalytic cycle (Scheme 1). Acyl-CoA dehydrogenase (ACD), which is an FAD-containing flavoenzyme and the mitochondrial counterpart of ACO, also catalyses the initial and rate-determining step of the mitochondrial fatty acid β-oxidation, *i.e.*, α,β-dehydrogenation of acyl-CoA into *trans*-enoyl-CoA in the reductive half-reaction. (The structure and numbering system of the flavin ring are presented in Fig. 1.) In contrast to ACO, the reduced form of ACD is reoxidized in the oxidative half-reaction by electron-transferring flavoprotein (ETF), from which the electrons are transferred to the mitochondrial respiratory chain coupled with ATP synthesis. While the enzymes of the mammalian ACD family have been studied extensively with reference to their enzymatic and physicochemical properties as well as the three-dimensional struc-

[1]This study was supported in part by the following grants: Grants-in-Aid for Scientific Research on Priority Areas from the Ministry of Education, Science, Sports, and Culture of Japan [B: 13125207 (K.H.), and 13125206 (R.M.)], and Research Grants from the Japan Society for the Promotion of Science [Category B: 13480196 (K.H.)], and Sakabe Project of Tsukuba Advanced Research Alliance (K.H.). Coordinates for ACO-II have been deposited in the RSCB Protein Data Bank as entry 1IS2.

[2]To whom correspondence should be addressed. E-mail: hirotsu@sci.osaka-cu.ac.jp, Fax: +81-6-6605-3131.

Abbreviations: ACO, acyl-CoA oxidase; ACD, acyl-CoA dehydrogenase; ETF, electron-transferring flavoprotein; MIRAS, multiple isomorphous replacement with anomalous scattering; ASA, accessible surface area; MCAD, medium-chain acyl-CoA dehydrogenase; rms, root mean square; Thr326*, the asterisk (*) indicates a residue from the other subunit of the dimeric molecule.

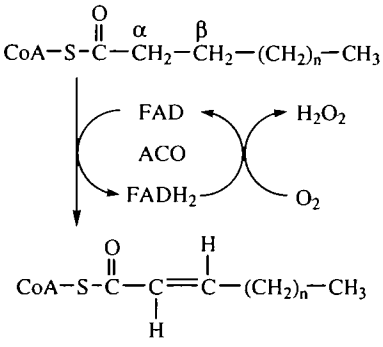

Scheme 1

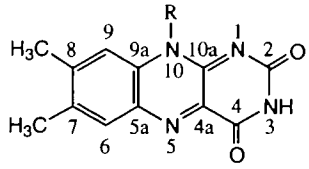

Fig. 1. **The structure and numbering system of the flavin ring of FAD.**

tures, the studies on mammalian ACOs are relatively limited and have not addressed their three-dimensional structures, even though ACD and ACO belong to the same superfamily (for a recent review of β-oxidation systems including ACD and ACO, see Ref. *1*). While mitochondrial ACDs are generally homotetramers of a subunit of 40–45 kDa (*2*), rat liver ACO is a homodimer of a subunit comprising 661 amino acids with the molecular mass of 75 kDa (*3, 4*). The N-terminal portion up to 440 amino acid residues of rat ACO corresponds to the ACD family; the primary structure of ACO is characterized by an N-terminal region corresponding to the ACD family to which a tail of 221 amino acid residues is attached. It has been postulated that ACO deploys Glu421 as the catalytic base to abstract the substrate α-proton on the basis of the sequence alignment of ACD family and ACO (*2*); Glu421 corresponds to the catalytic base, Glu376, of medium-chain acyl-CoA dehydrogenase (MCAD), one of the most extensively investigated ACDs with a known three-dimensional structure (*5*). However, this postulation has not been proved experimentally or structurally.

Though the purification of rat liver ACO and its properties were first described by Osumi *et al.* (*3*), their preparation seemed to be heterogeneous, consisting of intact and cleaved proteins of the two forms of the enzyme; the occurrence of two forms of rat ACO had been implicated by nucleotide sequence studies (*4, 6*). We have recently expressed two forms (ACO-I and ACO-II) of rat liver ACO and obtained them separately in pure forms (*7*). The two forms exhibit different substrate specificities, ACO-I showing optimal activity toward shorter acyl chain-length with maximum at C10 than ACO-II with maximum at C14 (*7*). Difficulty in purifying ACO from animal organs due to proteolytic cleavage in addition to the presence of isoforms has hampered the detailed analysis of the enzymatic and spectroscopic properties as well as structural analysis. Taking advantage of the expression system of the recombinant enzymes, we have studied the ligand-flavin interaction in ACO-I and -II and discussed differences and similarities between the two isoforms as well as between ACO and MCAD (*8*). The members of the ACD family show different substrate specificity from one another in terms of chain-length, branching, or charged state of the acyl moiety, *e.g.*, MCAD exhibits the optimum activity with straight acyl-chain of C8-C10 (*9*). The three-dimensional structure of ACO has long been awaited not only for understanding the molecular details of the catalysis of ACO itself but also for the knowledge of the generalization of the ACD-ACO superfamily in the reductive half-reaction and for knowing the mechanism of the reactivity toward oxygen in the oxidative half-reaction. In our recent study on the crystal structure of an intermediate for the oxidative half-reaction of D-amino acid oxidase, we proposed a generalized scheme for controlling the reactivity of reduced flavoenzyme toward oxygen (*10*). ACD and ACO make up an excellent pair in verifying this generalized scheme for the reactivity of the reduced form of flavoenzyme toward molecular oxygen, since they differ only in the oxidative half-reaction; reduced ACD reacts with ETF instead of oxygen, whereas reduced ACO reacts with oxygen. We report herein the three-dimensional structure of rat liver ACO-II which provides the first structure ever for acyl-CoA oxidase.

MATERIALS AND METHODS

Crystallization and Data Collection—The expression of ACO-II by *Escherichia coli*, the purification of the expressed enzyme, and the crystallization of native ACO-II together with preliminary crystallographic analysis have been reported elsewhere (*11, 12*). Briefly, crystallization for ACO-II was carried out at 293 K by the hanging-drop vapor-diffusion method using PEG20000 as the precipitant (*13*). A droplet of 10 μl of protein solution [2.0 mg/ml protein solution, 3.0% (w/v) PEG20000, 20 mM potassium phosphate, pH 7.4] was equilibrated against 400 μl of reservoir solution [8–11% (w/v) PEG20000, 100 mM potassium phosphate, pH 7.4]. After about a week, yellow crystals had grown to dimensions of 0.3 × 0.2 × 0.5 mm, which belonged to a space group $P2_12_12_1$ with the following cell dimensions: a = 72.0, b = 91.5, c = 214.5 Å. One dimer molecule is found in the asymmetric unit, and 48% of the crystal volume is occupied by solvent. The native X-ray diffraction data was collected to 2.2 Å resolution at 100 K on the BL41XU station at Spring-8 (Hyogo), using an X-ray beam with a wavelength 1.0 Å and MAR CCD165 detector, and processed and scaled by HKL2000 (Table I) (*14*). Before flash freezing, all the crystals were soaked for a few seconds in a solution containing 30% PEG400, 11% PEG20000, 100 mM potassium phosphate pH 7.4. The data sets for the crystals soaked in 0.1 mM chloromethylmercury for 4 h and 0.1 mM *p*-chloromercuribenzene sulfonate for 2 h were collected to 2.6 Å resolution at 100 K on the same station of SPring-8 and 2.8 Å resolution at 100 K on the BL18B station at the Photon Factory (Tsukuba), respectively. The former data were processed and scaled by HKL2000 (*14*), and the latter by MOSFLM and SCALA (*15*).

Structure Determination and Refinement—The structure of ACO-II was solved by the MIRAS (multiple isomorphous replacement with anomalous scattering) method (*16*), using two isomorphous data sets. The scaling of all data and map calculations were performed with CCP4 program suite (*17*).

TABLE I. **Data collection, MIR, and refinement statistics.**

	Native	CH_3HgCl	PCMBS[a]
Data collection			
Space group	$P2_12_12_1$	$P2_12_12_1$	$P2_12_12_1$
Lattice parameter (Å)			
a	72.0	71.9	71.0
b	91.5	91 4	87.6
c	214.5	214.3	213.0
Temperature (K)	100	100	100
Wavelength (Å)	1.00	1.02	1.00
Resolution range (Å)	20.0–2.20 (2.27–2.20)	20.0–2.60 (2.69–2.60)	20.0–2.80 (2.95–2.80)
No. of reflections			
Observation	344,046 (22,267)	200,374 (17,452)	125,745 (16,325)
Unique	69,647 (6,152)	44,225 (4,384)	32,497 (4,594)
Completeness (%)	94.7 (85.3)	99.8 (99.9)	97.2 (95.0)
R_{merge}[b] (%)	6.0 (28.3)	6.8 (13.9)	7.0 (15.4)
Mean $I/\sigma(I)$	16.0 (2.1)	18.7 (8.4)	7.4 (4.6)
MIR			
R_{diff}[c] (%)		18.4	22.4
Phasing power[d]		1.6	0.7
No. of sites		4	2
Refinement			
Resolution limit (Å)	10.0–2.2		
R_{factor} (%)	20.9		
R_{free} (%)	26.0		
Deviations			
Bond lengths (Å)	0.007		
Bond angles (deg)	1.3		
B factors			
avg main chains (Å^2)	31.7		
avg side chains (Å^2)	33.6		
avg cofactors (Å^2)	38.9		
avg waters (Å^2)	35.7		

[a]PCMBS: *p*-chloromercuribenzene sulfonate. [b]$R_{merge} = \Sigma_{hkl}\Sigma_i|I_{hkl,i}-\langle I_{hkl}\rangle|/\Sigma_{hkl}\Sigma_i I_{hkl,i}$, where I = observed intensity and $\langle I\rangle$ = average intensity for multiple measurements. [c]$R_{diff} = \Sigma||F_{PH}|-|F_P||/\Sigma|F_P|$, where $|F_{PH}|$ and $|F_P|$ are the derivative and native structure factor amplitudes, respectively. [d]Phasing power is the ratio of the root-mean-square (rms) of the heavy atom scattering amplitude and the lack of closure error.

The difference Patterson map calculations for chloromethylmercury and *p*-chloromercuribenzene sulfonate allowed clear interpretation of four and two mercury sites, respectively. Refinement of the heavy atom parameters and calculations of the initial phases were performed with the program SOLVE (*18*). The resulting MIRAS map has a mean figure of merit of 0.52. The map was improved by the process of solvent flattening with the program RESOLVE (*18*) to give a mean figure of merit of 0.69. The model of one subunit (subunit 1) and FAD was gradually built into 3.0 Å map through several cycles of model building using the program O (*19*). That of the other subunit (subunit 2) and FAD in the asymmetric unit were obtained by taking advantage of a local 2-fold axis.

The structure of ACO-II was first refined by simulated annealing and energy minimization with 2-fold noncrystallographic symmetry restraints with the program CNS (*20*), using X-ray data from 10 to 2.5 Å resolution. However, R_{factor} and R_{free} were not reduced below 28.1 and 40.7% respectively. At this stage, the restraint on 2-fold noncrystallographic symmetry was removed, and the entire molecule was refined. The structure was scrutinized by inspecting the composite omit map. After several rounds of refinement and manual rebuilding, R_{factor} and R_{free} were reduced to 25.7 and 33.7%, respectively. The resolution was increased to 2.2 Å resolution, and refinement by simulated annealing and rebuilding was alternated until no further improvements in structure and statistics were apparent with R_{factor} = 23.2%, R_{free} = 30.3%. Water molecules were picked up on the basis of the peak height and the distance criteria from the difference map. The water molecules whose thermal factors were above 70 Å^2 (maximum thermal factor of the main chain) after refinement were removed from the list. Further model building and refinement cycles resulted in an R_{factor} of 20.6 % and R_{free} of 26.0%, using 67,164 reflections [$F_o > 2\sigma(F_o)$] between 10.0 and 2.2 Å resolution (Table I). The maximum thermal factor of water molecules was 69 Å^2.

Quality of the Structure—The refined model comprises 637 residues for subunit 1, 629 residues for subunit 2, two FADs, and 443 water molecules. This model lacks the 24 residues for subunit 1 (Pro268–Asn271, Gln461–Met474, and C-terminal six residues) and 32 residues for subunit 2 (Pro268–Thr277, Pro459–Met474, and C-terminal six residues) due to no interpretable electron density. Alanine models were applied for Lys272, Glu316, Val475, His508-Arg509, Lys512, Glu648, Lys652, and Lys655 in subunit 1, and Asp81, Glu83, Met86, His113-Gln114, Glu118–Glu121, Met125, Trp128-Asn129, Lys255, Asp262, Lys267, Phe280, Arg346, Lys446, His508, Lys510, Glu630, Glu648, and Lys655 in subunit 2, since the electron densities corresponding to the side-chains of these residues located on the molecular surface were weak or not observed. The average thermal factors of the main chain atoms in subunits 1 and 2 are 29.5 and 33.9 Å^2, respectively, and the maximum ones in subunits 1 and 2 are 61.6 and 71.0 Å^2.

Analysis of the stereochemistry with PROCHECK (*21*) showed that all the main chain atoms except for Trp176 for subunits 1 and 2 fall within the generously allowed region

of the Ramachandran plot with 1,035 residues in the most favored region and 75 in the additionally allowed region. On the basis of the electron density map, it is confirmed that the conformation of Trp176 residue in subunits 1 or 2 is correct. Structure diagrams were drawn with programs Molscript (*22*), Bobscript (*23*), and Raster3D (*24*).

RESULTS AND DISCUSSION

Overall Structure—The overall structure of ACO-II and the dimeric unit of MCAD perpendicular to the molecular two-fold axis are shown in Fig. 2. The main-chain Cα atoms of MCAD from pig liver mitochondria in the free uncomplexed form can be superimposed on those of MCAD in complex with octanoyl-CoA (*5*), butyryl-CoA dehydrogenase from *Megasphaera* in complex with acetoacetyl-CoA (*25*), and T255E/E376G mutant of human MCAD in the uncomplexed and complexed forms (*26*) within rms deviations of 0.16–0.68 Å by the least-squares method, indicating that the overall and active site structures are quite similar among these dehydrogenases irrespective of whether the enzymes are uncomplexed or complexed forms. We use MCAD as a reference standard for ACDs for comparison with ACO-II. DALI calculation (*27*) shows that MCAD has Z-score of 28.9 and the sequence identity of 20.9% with the residues from His21 to Asp440 of ACO-II. When C-terminal 221 residues of ACO-II are omitted, the overall fold of ACO-II is similar to that of a dimer unit (active one) in tetrameric MCAD (*5*), but the overall structure is distinguishable (Fig. 2). The residues from Glu441 to Ala590 out of the C-terminal 221 residues occupy the contact region observed between two dimeric units of MCAD, and pack against the 2-fold related part of the other subunit, preventing ACO-II from forming a tetramer found in MCAD. The residues from Arg591 to Leu661 of the C-terminus extend and reach the backside of the active site of the other subunit. The ASAs (accessible surface area) of ACO-II and its subunit interface are 45,204 and 10,726 Å^2, respectively. The ASA of the subunit interface of the dimeric unit in MCAD is 4,106 Å^2, which is compared with 4,619 Å^2 observed in the corresponding region in ACO-II.

Subunit Structure—The α-carbon atoms of the subunits 1 and 2 were superimposed by the least-squares method,

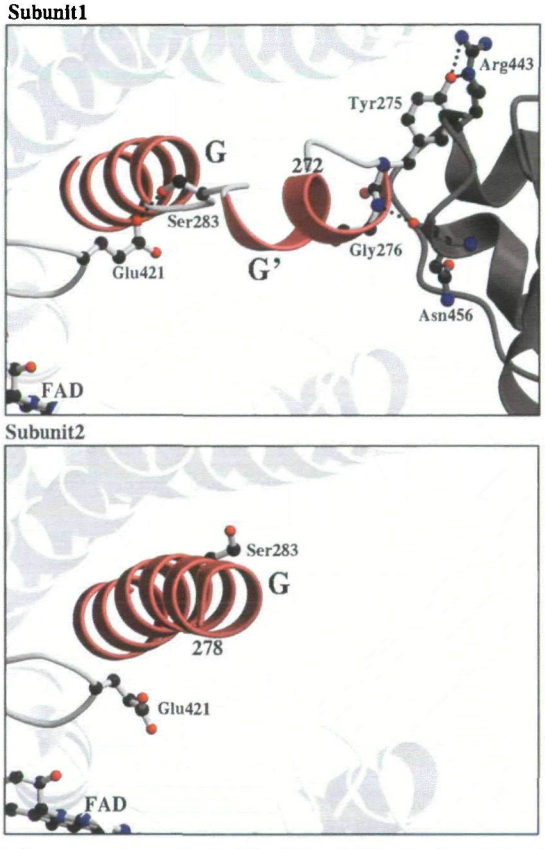

Fig. 3. **A comparison of α-helix G (and G') of subunit 1 with α-helix G of subunit 2 in ACO-II.** The α-helix G (and G') and its surroundings are shown in red and light gray, respectively. The hydrogen bonds are shown by dotted lines. The neighboring molecule in the crystal is drawn in dark gray. In subunit 1, the α-helix G is deformed by the intermolecular hydrogen bonds between Tyr275 and Arg443, and between Gly276 and Asn456, resulting in the rearrangement of Ser283 to interact with the catalytic Glu421.

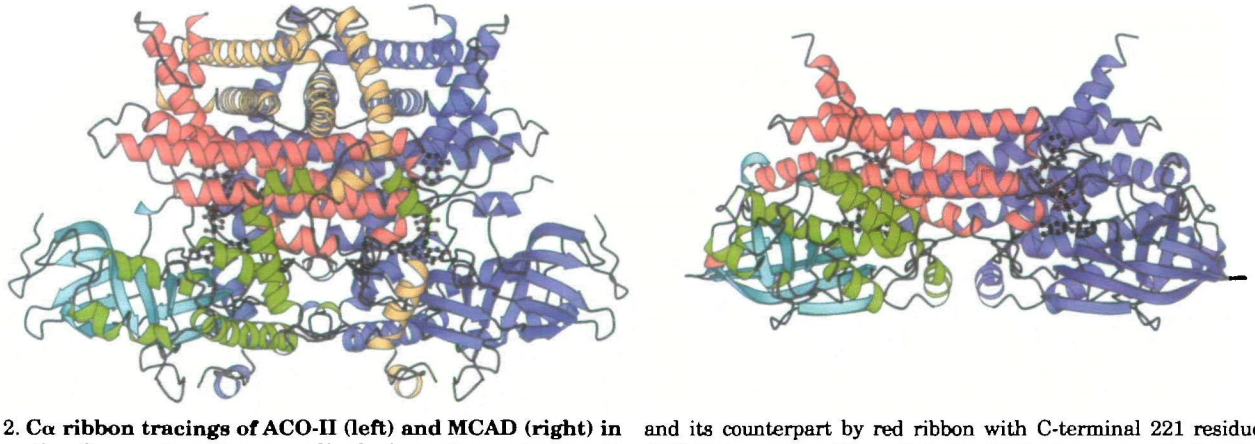

Fig. 2. **Cα ribbon tracings of ACO-II (left) and MCAD (right) in the native forms viewed perpendicularly to the molecular 2-fold axis.** One subunit of ACO-II or MCAD is represented by blue ribbon. The N-terminal α-domain and β-domain in the other subunit of ACO-II or MCAD are shown by green and cyan ribbons, respectively, and the first 169 residues of C-terminal α-domain of ACO-II and its counterpart by red ribbon with C-terminal 221 residues of ACO-II in orange ribbon. Cofactor FAD, shown as a ball-and-stick model, is bound to the large crevice between the β- and C-terminal α-domains of one subunit, and the C-terminal domain of the other subunit.

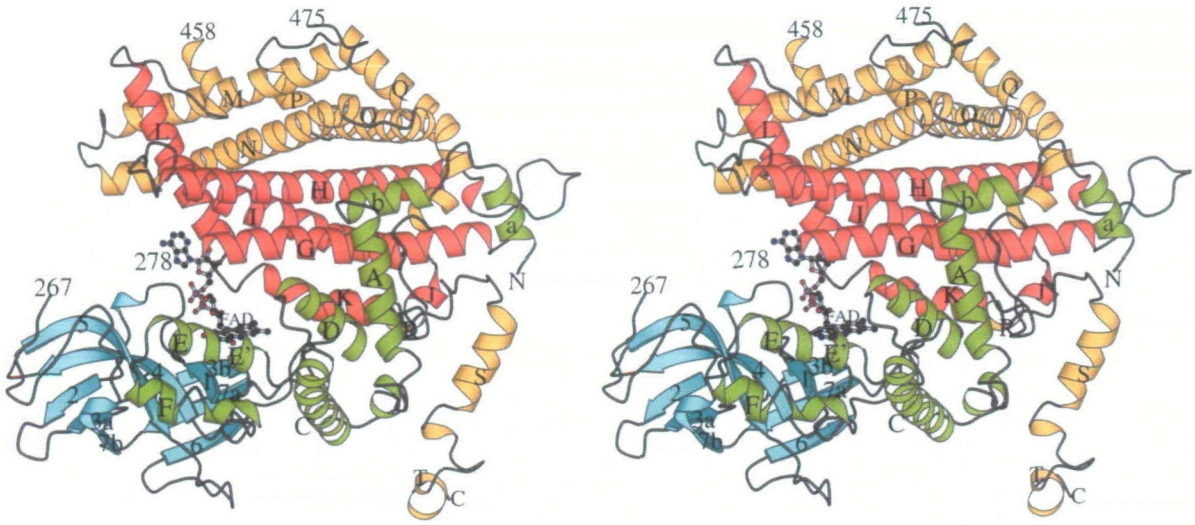

Fig. 4. **Stereoview of the subunit of ACO-II structure with secondary structure assignments.** α-Helices are denoted as a, b, A, C–F in the N-terminal α-domain (green), and G–U in the C-terminal α-domain (red for G–L, and orange for M–T). β-Strands are denoted as 1–7b in the β-domain (cyan). The cofactor FAD is drawn as a ball-and-stick model. The numbering of helices and strands of ACO-II follows that in MCAD.

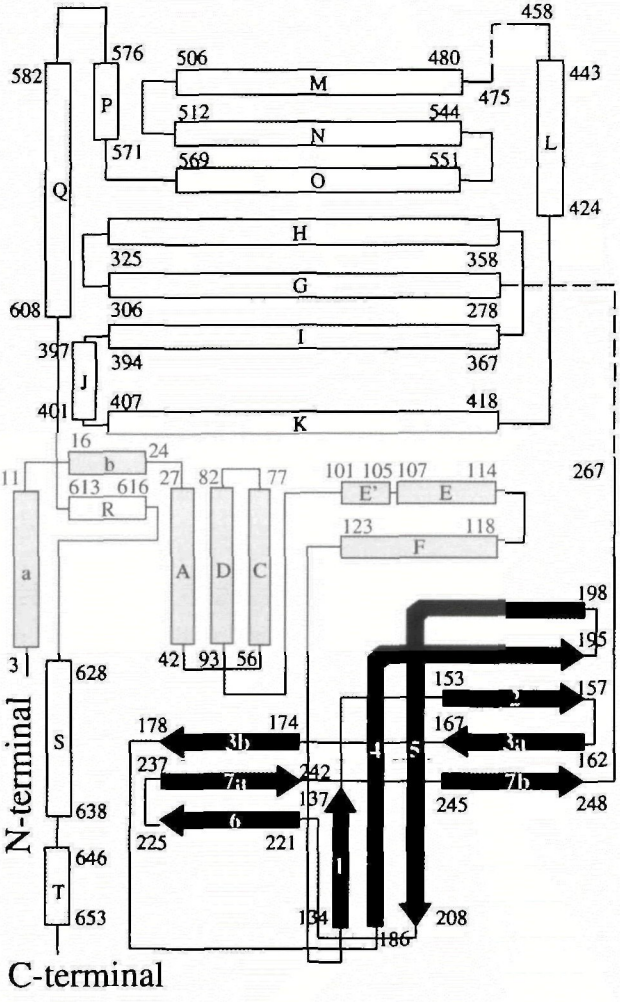

Fig. 5. **Topological diagram showing the secondary structure of ACO-II.** The N- and C-terminal domains are represented by the shaded and open α-helices, respectively, and the β-domain by full strands.

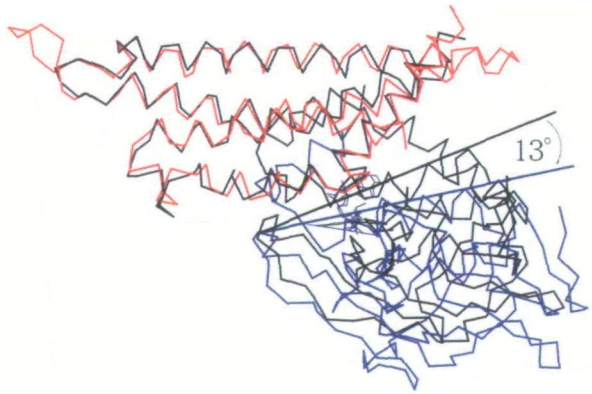

Fig. 6. **Superposition of ACO-II onto MCAD by least-squares fitting of Cα-atoms in C-terminal α-domains.** The black line represents MCAD, and the red and blue lines represent the C-terminal α-domain and the N-terminal α-domain plus the β-domain in ACO-II, respectively. The N-terminal α-domain and the β-domain of ACO-II show the 13° rotation with respect to the C-terminal α-domain compared with those in MCAD to widen the crevice for substrate binding.

showing that there are apparent deviations amounting to 5.9–8.0 Å around the region from Met278 to Ser283. The residues from Met278 to Val306 make up α-helix G in subunit 2, while the same region forms α-helix G′ (275–281), a loop (282–284), and α-helix G (285–306) in subunit 1 (Fig. 3). Tyr275 and Gly276 of subunit 1, which are not visible in subunit 2, form hydrogen bonds with Arg443 and Asn456 of a neighboring dimer molecule, respectively, probably inducing the large shift of Met278 to Ser283 toward the N-terminal direction of α-helix G. In addition, this deformation of α-helix G in subunit 1 affects the orientation of Glu421, the catalytic residue, as discussed later. This is a case where intermolecular interactions alter the protein folding and the active site structure, although the deformation is relatively local. The main chain Cα atom of Glu421 in subunit

1 is moved by 1.0 Å and the direction of its side-chain is directed away from the flavin ring by forming a hydrogen bond with the Ser283 hydroxyl group. We use subunit 2 hereafter as the reference standard in the following discussion, since the structure of subunit 1 is affected by the crystallographic artifactual intermolecular interactions, which makes Glu421 in subunit 1 unsuitable for catalysis.

The subunit structure and the topology diagram of ACO-II are shown in Figs. 4 and 5, respectively, with the secondary structure assignment by the program DSSP (*28*). The subunit is divided into N-terminal α-domain (N-terminus to Ile132), β-domain (Tyr133 to Leu269), and C-terminal α-domain (Ser270 to C-terminus) (Fig. 4). The β-domain is located between the N-terminal α-domain and C-terminal α-domain to interconnect these two domains. The N-terminal α-domain consists of seven α-helices where the antiparallel α-helices A, C, D, E′-E, and F pack together. The α-helices A, C, and F are on the side of the molecular surface, while D and E′-E are inside the molecule to form a part of the active-site crevice for binding the fatty acyl chain of a substrate. The α-helices a and b extend toward the C-terminal α-domain and cover its surface. In the β-domain, the three-stranded antiparallel β-sheet (3b, 6, and 7a) is connected to the six stranded β-sheet (1, 2, 3a, 4, 5, and 7a) through the polypeptide chains between strands 3a and 3b, and 7a and 7b, forming an elongated pseudo β-barrel. One side of the β-barrel is situated on the molecular surface, while the other side faces the active-site crevice and participates in the interaction with the flavin ring of FAD. The C-terminal α-domain is made up of nine α-helices and loops connecting them. The α-helices G, H, I, and K form a four-helix bundle with short α-helix J between α-helices I and K. α-Helices G and K are involved in the formation of the crevice for the fatty acyl chain of a substrate. The bundle is linked through α-helix L to another cluster of four α-helices of M, N, O, and Q arranged in nearly the same direction. This cluster protects the four-helix bundle from the solvent. The region corresponding to the cluster of α-helices M, N, O, and Q is within the C-terminal tail which is absent in ACDs.

Using the result of DALI calculation (*27*), the corresponding Cα atoms between ACO-II and MCAD are fit within an rms deviation of 1.37 Å with a maximum displacement of 6.9 Å, while the Cα atoms of the N-terminal α-domain plus the β-domain, and those of the C-terminal α-domain in ACO-II can be superimposed onto the corresponding ones in MCAD within rms deviations of 0.87 and 0.60 Å with the maximum displacements of 4.71 and 2.57 Å, respectively. Roughly, the relative location of the domains in ACO is different from that in MCAD. The N-terminal α- and the β-domains of ACO-II are rotated by 13° from the location of the corresponding domains in MCAD with the loop between β-strands 6 and 7a acting as the hinge, resulting in a much wider crevice for the substrate in ACO-II than that in MCAD (Fig. 6). These observations suggest that ACO-II may change its conformation from an open to a closed form upon binding a substrate (*29, 30*). However, the MCAD and other ACDs so far determined by X-ray methods do not undergo such conformational change (*5, 26*).

FAD Binding—The $2F_o$–F_c electron density map for FAD and some residues surrounding FAD is shown in Fig. 7. FAD is bound to the bottom of the large crevice between the β-domain and the four-helix bundle of the C-terminal domain with its *si*-face of the flavin ring oriented toward the β-domain (Fig. 4). This geometry of FAD-binding establishes the *re*-face specificity of the flavin ring for the catalytic event of ACO-II. Both subunits of the dimer molecule are involved in the FAD binding. The adenosine diphosphate portion of FAD is recognized by hydrogen bonds with both subunits of the dimer, whereas the riboflavin moiety interacts mostly with only one subunit through hydrogen bonds.

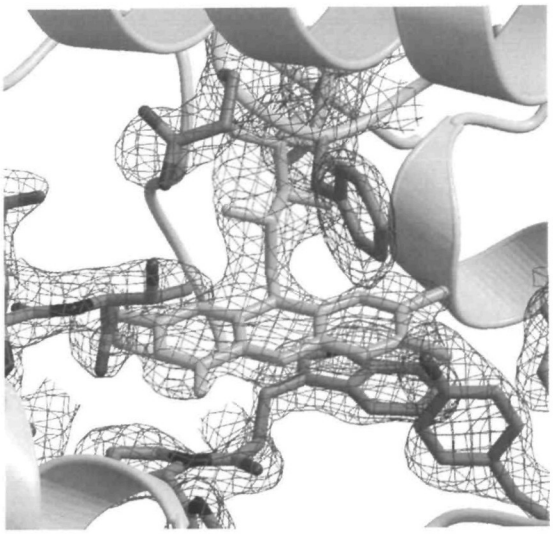

Fig. 7. **The $2F_o$–F_c electron density map of ACO-II calculated using 8.0–2.2 Å resolution for FAD and some residues close to FAD.**

The adenosine moiety of FAD interacts with one side of the four-helix bundle in one subunit (the loop between α-helices K and L), and with the other side of the helix bundle from the other subunit (the loop between α-helices H and G, and N- and C-terminal regions of α-helices H and I). Thus, the dimer formation is essential for FAD binding. The pyrophosphate group of FAD interacts with the loop between the β-strands 1 and 2 of one subunit, and the C- and N-terminal regions of α-helices G and J of the other subunit. The negative charge of the pyrophosphate is well balanced with the positive charge of Arg307* (* means the residue from the other subunit of the molecule) and the positive end of the dipole of α-helix J of the other subunit. The binding mode of the adenosine diphosphate moiety in ACO-II is fairly similar to that in MCAD; the binding site is located in the subunit interface whose structure is not affected by the difference in the relative location of domains (Fig. 2). On the other hand, the binding site for the flavin ring reflects the difference of the relative orientations of the domains as described below.

The *si*-face of FAD directs toward Trp176 and Pro177 of β-strand 3b (Fig. 8a). The indole and pyrrolidine rings of these residues are nearly coplanar, making a parallel stack with flavin, and covering the *si*-face of the flavin ring. The distance between these two planes with flavin is 3.6–3.8 Å. The amide NH of Gly178 forms a weak hydrogen bond with C(4)=O of flavin: the distance of N—O is 3.3 Å, and the angle of N—O=C is 116°. Tyr232 of the N-terminal loop region of β-strand 7a and Tyr401* of α-helix J of the other

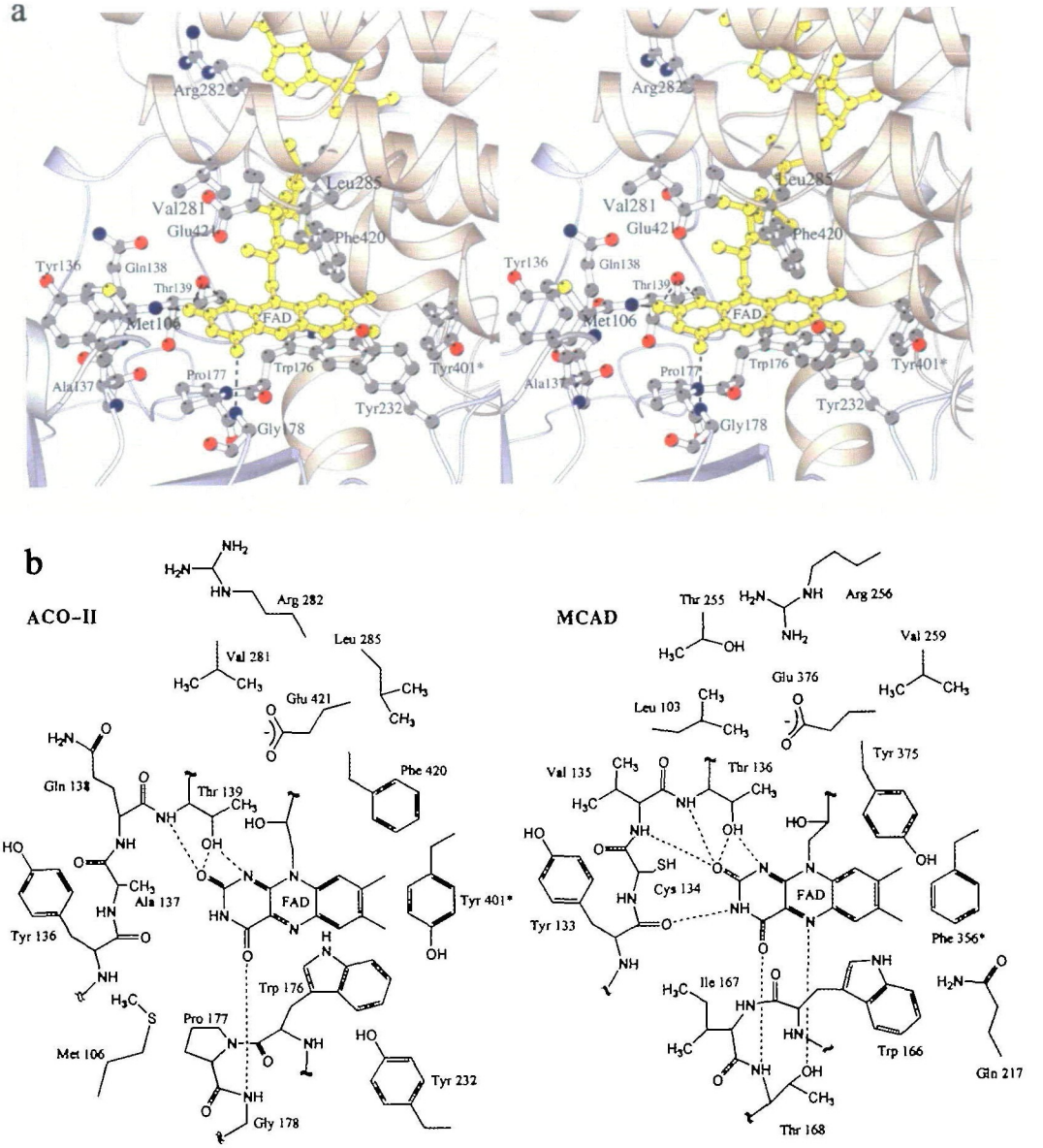

Fig. 8. **(a) Stereoview of the active site in ACO-II from the solvent side.** β-Domain and N-terminal α-domain are displayed by pale gray and orange ribbons, respectively. The active site residues and FAD (yellow) are drawn as a ball-and-stick model. Putative hydrogen bonds between the flavin ring and the active site residues are shown by dotted lines. **(b) Schematic diagrams showing hydrogen-bonding interactions in ACO-II (left) and MCAD (right).** Putative interactions are shown by dotted lines if the acceptor and donor less than 3.5 Å apart. The asterisk (*) after the residue number indicates a residue from another subunit of the molecule.

subunit have access to the C(7) methyl group and C(7) and C(8) methyl groups of flavin, respectively. The pyrimidine moiety of flavin is approached by Tyr136, Ala137, Gln138, and Thr139 of the C-terminal region of β-strand 1. However, only Thr139 forms hydrogen bonds with N(1) and C(2)=O of flavin. Phe420 on the loop between α-helices K and L hangs over the xylene moiety of flavin with the approximately perpendicular orientation to each other. In addition to Phe420, Glu421 resides over the pyrimidine portion with its carboxylate group at 6.2 Å from the flavin ring. Glu421 has been postulated as the catalytic base for abstracting the α-proton from the substrate acyl portion on the basis of the sequence alignment among ACD family members and ACO (2). Our finding that the carboxylate group of Glu421 is located suitably for catalysis provides firm evidence for its role as the catalytic base. Moreover, no other amino acid residue candidates for the catalytic base are found within the vicinity of the flavin ring.

The Active Site Structure—The active site is defined as the flavin ring, the residues (Tyr136, Ala137, Gln138, Thr139, Trp176, Pro177, Gly178, Tyr232, and Tyr401*) interacting with the flavin ring, and the catalytic Glu421 residue and the surrounding residues (Val281, Arg282, Leu285, and Phe420), as shown in Fig. 8a. The hydrogen-bonding networks of the active sites of ACO-II and MCAD are displayed in Fig. 8b. The corresponding Cα atoms and the flavin ring in the active sites of ACO-II and MCAD are superimposable within an rms deviation of 0.46 Å except

for Val281, Arg282, Leu285, Phe420, Glu421, and their counterparts in MCAD. The Cα atoms of the residues excluded from the least-squares fitting shows the displacement of 1.6–3.4 Å, indicating that the active site structure of ACO-II is distinct from that of MCAD (Fig. 9). The arrangement of the flavin ring to the β-domain is similar in the two enzymes, whereas many residues surrounding the flavin ring in ACO-II deviate away from the corresponding ones. This deviation is mainly ascribed to the difference in the relative orientation of the domains in ACO-II from that in MCAD (see "*Subunit Structure*").

Out of the nine residues interacting with the flavin ring of ACO-II, only three residues, Tyr136, Thr139, and Trp176, are conserved in MCAD. N(1), C(2)=O, N(3)-H, C(4)=O, and N(5) of flavin in MCAD are involved in hydrogen bonds with the surrounding residues, while in ACO-II only three hydrogen bonds are associated with flavin at N(1), C(2)=O, and C(4)=O: N(1) and C(2)=O make hydrogen bonds with Thr139 hydoxy group, and C(4)=O with the main chain NH of Gly178. In ACO-II, the C-terminal region of β-strand 1 loosely interacts with the pyrimidine portion of flavin, due to the loss of hydrogen bonds present in MCAD in this region (Tyr136, Ala137, and Gln138) with C(2)=O and N(3)-H of flavin. Thr168, whose side-chain hydroxyl group is hydrogen bonded to N(5) of flavin in MCAD, is replaced by Gly178 in ACO-II, which lacks a side-chain capable of hydrogen bonding. Thus flavin N(5) of ACO-II is free from hydrogen bonding with the protein moiety. The accessible surface area (ASA) of the flavin ring in ACO-II is 32 Å^2, while that in MCAD is 12 Å^2 indicating that the flavin ring of ACO-II is less encapsulated within the protein compared with that of MCAD. The increased ASA of the flavin ring in ACO-II is in part due to the loose interaction of the β-strand 1 with flavin, and the replacement of Thr168 in MCAD by small Gly178 without hydrogen-bonding side chain. Moreover, the residues (Val281, Arg282, Leu285, and Phe420 of the C-terminal α-domain) hanging over the *re*-face of the flavin ring are significantly removed away from the flavin ring compared with the corresponding residues in MCAD. Consequently, the C(2)=O, N(3), C(4)=O, C(4a), and N(5) of ACO-II are exposed to the solvent and can be approached by molecular oxygen. In contrast, the access of molecular oxygen to C(4a) of MCAD is less feasible due to the close packing of the active site (*5*); oxidation of reduced flavin by oxygen is initiated by the nucleophilic attack of C(4a) of reduced flavin to oxygen.

No residues surrounding the catalytic residue, Glu421, in ACO-II are conserved in MCAD except Arg282, but the hydrophobic atmosphere around the catalytic residue is a common feature for both enzymes. The active-site folding and the location of the flavin ring with respect to the β-domain are similar to those in MCAD. The catalytic residue to abstract the α-proton and the arginine residue to recognize C(5)=O of the CoA moiety in MCAD are conserved in ACO-II, implying that the mode of substrate binding is similar between the two enzymes; the Cα-Cβ bond of the substrate is sandwiched between the flavin ring and the catalytic residue, Glu421. However, the active-site residues from the C-teminal α-domain are remote from the flavin ring compared with those in MCAD. The distance between the Cα atom of Glu421 and N(10) of the flavin ring in ACO-II is 7.8 Å, which is longer by 0.9 Å than that in MCAD. In order for the α-proton of the substrate to be eliminated, the Cα atom of Glu421 should move toward the flavin ring upon substrate binding. For this movement of the Glu421 Cα, the four-helix bundle of the C-terminal needs to move to close the active site. In order to confirm the existence or nonexistence of the open-closed conformational change, however, we must await the X-ray structure determination of ACO-II in complex with a substrate (analog) or an inhibitor.

Binding Site for Fatty Acyl Chain—The long and wide crevice for binding the fatty acyl chain is formed by Tyr232, α-helices D, and E′-E along with the loop between them, α-helix G, and α-helix K. The end of the crevice is made up of the loop between α-helices Q and R, and the succeeding α-helix R, suggesting that the C-terminal region of ACO-II, whose counterpart is absent in MCAD, plays an important

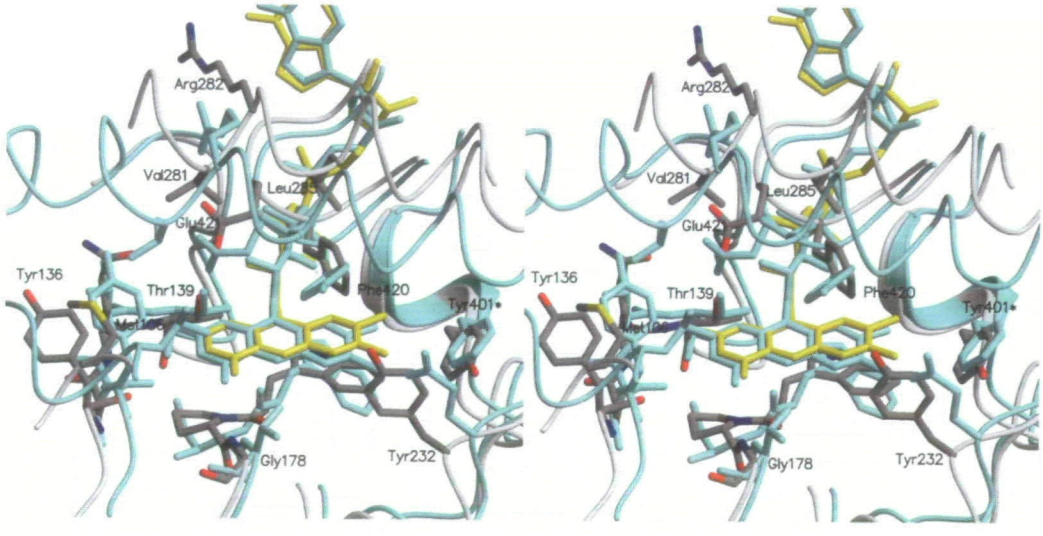

Fig. 9. **Superposition of the active site residues and FADs between ACO-II (side chains in dark gray, main chains in gray, and FAD in yellow) and MACD (cyan).** The main chain loops bearing Thr139, Tyr232, and Glu421 in ACO-II are away from the corresponding loops in MACD.

role in substrate binding. The crevice is about 28 Å long and 6 Å wide, and can accommodate the straight acyl chain of C23 in length. ACO-II shows the maximum activity for C14 acyl chain-length and the lower activity for the longer chain acyl-CoAs (*7*). This may stem from the narrowing (about 4 Å) of the crevice formed by Asn90, Gln291, and Lys295 at about 18 Å from the entrance.

Mechanistic Implications—Since the active-site structure of ACO-II is essentially the same as that of MCAD, the binding mode of substrate acyl-CoA in ACO-II resembles that in MCAD; the reductive half reaction (oxidation of the substrate and reduction of FAD) proceed *via* the α-proton abstraction by the catalytic base (Glu421 in ACO-II or Glu376 in MCAD) in concert with hydride transfer from the substrate β-position to flavin N(5) (*31*). What differentiates ACO-II as an oxidase from MCAD as a dehydrogenase is the remaining and the mechanistically most important question. In MCAD, the flavin ring of FAD is shielded from solvent and protected from the attack of molecular oxygen, irrespective of whether the enzyme is free or in complex with a substrate (*5*). In contrast, the flavin ring of ACO-II is found in a relatively large cavity, thus facilitating the access of molecular oxygen. Furthermore, the pyrimidine moiety of the flavin ring in ACO-II is exposed to solvent and readily accessible to molecular oxygen. The three-dimensional structure of ETF, the physiological electron acceptor of MCAD, has recently been solved and the model of ETF-MCAD complex has been deduced on the basis of the crystallographic structures of ETF and MCAD (*32*). According to this complex model, the ETF binding site is located above the *si*-face of flavin of MCAD. In ACO, however, the *si*-face of flavin is covered by the C-terminal α-helix S, protecting the *si*-face from access of ETF or other proteinous electron acceptor. From the three-dimensional structure of ACO-II, the oxidase nature of this enzyme can now be explained by physical inaccessibiliy of ETF or other proteinous electron acceptor for electron acceptance from ACO-II as well as by accessibility of molecular oxygen to the flavin ring of ACO-II. However, the precise oxidase nature of ACO must await further crystallographic studies of the enzyme in the reduced form or in the intermediary state prior to the oxidative half-reaction.

REFERENCES

1. Kunau, W.-H., Dommes, V., and Schulz, H. (1995) β-Oxidation of fatty acids in mitochondria, peroxisomes, and bacteria: A century of continued progress. *Prog. Lipid Res.* **34**, 267–342
2. Matsubara, Y., Indo, Y., Naito, E., Ozasa, H., Glassberg, R., Vockley, J., Ikeda, Y., Kraus, J., and Tanaka, K. (1989) Molecular cloning and nucleotide sequence of cDNAs encoding the precursors of rat long chain acyl-coenzyme A, short chain acyl-coenzyme A, and isovaleryl-coenzyme A dehydrogenases. Sequence homology of four enzymes of the acyl-CoA dehydrogenase family. *J. Biol. Chem.* **264**, 16321–16331
3. Osumi, T., Hashimoto, T., and Ui, N. (1980) Purification and properties of acyl-CoA oxidase from rat liver. *J. Biochem.* **87**, 1735–1746
4. Miyazawa, S., Hayashi, H., Hijikata, M., Ishii, N., Furuta, S., Kagamiyama, H., Osumi, T., and Hashimoto, T. (1987) Complete nucleotide sequence of cDNA and predicted amino acid sequence of rat acyl-CoA oxidase. *J. Biol. Chem.* **262**, 8131–8137
5. Kim, J.J.-P., Wang, M., and Paschke, R. (1993) Crystal structures of medium-chain acyl-CoA dehydrogenase from pig liver mitochondria with and without substrate. *Proc. Natl. Acad. Sci. USA* **90**, 7523–7527
6. Osumi, T., Ishii, N., Miyazawa, S., and Hashimoto, T. (1987) Isolation and structural characterization of the rat acyl-CoA oxidase gene. *J. Biol. Chem.* **262**, 8138–8143
7. Setoyama, C., Tamaoki, H., Nishina, Y., Shiga, K., and Miura, R. (1995) Functional expression of two forms of rat acyl-CoA oxidase and their substrate specificities. *Biochem. Biophys. Res. Commun.* **217**, 482–487
8. Tamaoki, H., Setoyama, C., Miura, R., Hazekawa, I., Nishina, Y., and Shiga, K. (1997) Spectroscopic studies of rat liver acyl-CoA oxidase with reference to recognition and activation of substrate. *J. Biochem.* **121**, 1139–1146
9. Ikeda, Y., Okamura-Ikeda, K., and Tanaka, K. (1985) Purification and characterization of short-chain, medium-chain, and long-chain acyl-CoA dehydrogenases from rat liver mitochondria. Isolation of the holo- and apoenzymes and conversion of the apoenzyme to the holoenzyme. *J. Biol. Chem.* **260**, 1311–1325
10. Mizutani, H., Miyahara, I., Hirotsu, K., Nishina, Y., Shiga, K., Setoyama, C., and Miura, R. (2000) Three-dimensional structure of the purple intermediate of porcine kidney D-amino acid oxidase. Optimization of the oxidative half-reaction through alignment of the product with reduced flavin. *J. Biochem.* **128**, 73–81
11. Setoyama, C., Tamaoki, H., Nishina, Y., Shiga, K., and Miura, R. (1995) Functional expression of two forms of rat acyl-CoA oxidase and their substrate specificities. *Biochem. Biophys. Res. Commun.* **217**, 482–487
12. Nakajima, Y., Miyahara, I., Hirotsu, K., Nishina, Y., Shiga, K., Setoyama, C., Tamaoki, H., and Miura, R. (2001) Crystallization and preliminary X-ray characterization of rat liver acyl-CoA oxidase. *Acta Crystallogr.* **D57**, 1680–1681
13. Jancarik, J. and Kim, S.-H. (1991) Sparse matrix sampling: a screening method for crystallization of proteins. *J. Appl. Crystallogr.* **24**, 409–411
14. Otowinowski, Z. and Minor, W. (1997) Processing of X-ray diffraction data collected in oscillation mode. *Methods Enzymol.* **276**, 307–326
15. Leslie, A.G.W. (1992) *Joint CCP4 and ESRF-EESF-EACMB Newsletter on Protein Crystallography*, SERC Daresbury Laboratory, Warrington, UK
16. Drenth, J. (1999) *Principles of Protein X-Ray Crystallography (Second Edition)*, Springer-Verlag, New York
17. Collaborative Computational Project Number 4 (1994) The CCP4 suite: programs for protein crystallography. *Acta Crystallogr.* **D50**, 760–763
18. Terwilliger, T.C. and Berendzen, J. (1999) Automated structure solution for MIR and MAD. *Acta Crystallogr.* **D55**, 849–861
19. Jones, T.A., Zou, J.-Y., Cowan, S.W., and Kjeldgaard, M. (1991) Improved methods for building protein models in electron density maps and the location errors in these models. *Acta Crystallogr.* **A47**, 110–119
20. Brunger, A.T., Adams, P.D., Clore, G.M., DeLano, W.N., Gros, P., Grosse-Kunstleve, R.W., Jiang, J.-S., Kuszewski, J., Nilges, M., Pannu, N.S., Read, R.J., Rice, L.M., Simonson, T., and Warren, G.L. (1998) Crystallography & NMR system: A new software suite for macromolecular structure determination. *Acta Crystallogr.* **D54**, 905–921
21. Laskowski, R.A., MacArthur, M.W., Moss, D.S., and Thornton, J.M. (1993) PROCHECK: a program to check the stereochemical quality of protein structures. *J. Appl. Crystallogr.* **26**, 283–291
22. Kraulis, P.J. (1991) MOLSCRIPT: a program to produce both detailed and schematic plots of protein structures. *J. Appl. Crystallogr.* **24**, 946–950
23. Esnouf, R.M. (1997) An extensively modified version of Molscript that includes greatly enhanced coloring capabilities. *J. Mol. Graph. Model.* **15**, 132–134
24. Merritt, E.A. and Murphy, M.E.P. (1994) Raster3D version 2.0: a program for photorealistic molecular graphics. *Acta Crystallogr.* **D50**, 869–873

25. Djordjevic, S., Pace, C.P., Stankovich, M.T., and Kim, J.J. (1995) Three-dimensional structure of butyryl-CoA dehydrogenase from *Megasphaera elsdenii*. *Biochemistry* **34**, 2163–2171
26. Lee, H.J., Wang, M., Paschke, R., Nandy, A., Ghisla, S., and Kim, J.J. (1996) Crystal structures of the wild type and the Glu376Gly/Thr255Glu mutant of human medium-chain acyl-CoA dehydrogenase: influence of the location of the catalytic base on substrate specificity. *Biochemistry* **35**, 12412–12420
27. Holm, L. and Sander, C. (1993) Protein structure comparison by alignment of distance matrices. *J. Mol. Biol.* **233**, 123–138
28. Kabsch, W. and Sander, C. (1983) Dictionary of protein secondary structure: pattern recognition of hydrogen-bonded and geometrical features. *Biopolymers* **22**, 2577–2637
29. Koshland, Jr., D.E. (1987) Evolution of catalytic function. *Cold Spring Harbor Symp. Quant. Biol.* **LII**, 1–7
30. Gertein, M., Lesk, A.M., and Chothia, C. (1994) Structural mechanisms for domain movements in proteins. *Biochemistry* **33**, 6739–6749
31. Ghisla, S., Thorpe, C., and Massey, V. (1984) Mechanistic studies with general acyl-CoA dehydrogenase and butyryl-CoA dehydrogenase: Evidence for the transfer of the β-hydrogen to the flavin N(5)-position as a hydride. *Biochemistry* **23**, 3154–3161
32. Roberts, D.L., Frerman, F.E., and Kim, J.J.-P. (1996) Three-dimensional structure of human electron transfer flavoprotein to 2.1-Å resolution. *Proc. Natl. Acad. Sci. USA* **93**, 14355–14360